Macromolecules

Article

Cite This: Macromolecules 2019, 52, 8312−8322

pubs.acs.org/Macromolecules

Qualitative Effect of the Polymerization Rate on the Nanoparticle Dispersion in Poly(methyl methacrylate)/Silica Nanocomposite Films

Che-Yi Chu,*[,†] Yen-Cheng Li,[‡] Guang-Way Jang,[‡] Ying-Chih Pu,[§] Meng-Zhe Chen,[†] and Pei-Yin Chen[‡]

[†]Department of Chemical Engineering, National Chung Hsing University, Taichung 402, Taiwan

[‡]Material and Chemical Research Laboratories, Industrial Technology Research Institute, Hsin-Chu 31040, Taiwan

[§]Department of Materials Science, National University of Tainan, Tainan 70005, Taiwan

Supporting Information

Downloaded via SYNCHROTRON RADIATION RESEARCH on January 10, 2020 at 10:44:55 (UTC).
See https://pubs.acs.org/sharingguidelines for options on how to legitimately share published articles.

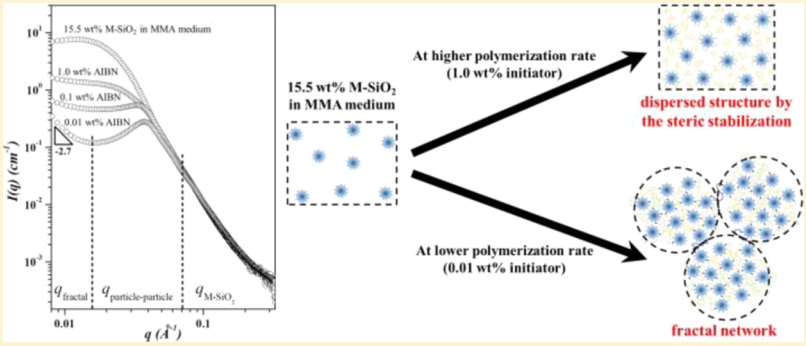

ABSTRACT: In this study, we investigate the effect of the polymerization rate, mainly mediated by the initiator concentration, on the nanoparticle dispersion in the nanocomposite films formed by poly(methyl methacrylate) (PMMA) and [3-(methacryloyloxy)propyl]trimethoxysilane-modified silica nanoparticles (M-SiO_2) via free radical polymerization of the precursory solution, that is, 15.5 wt % M-SiO_2 nanoparticles dispersed in the methyl methacrylate (MMA) monomer, in which the tethered silanes at the particle surface bearing the reactive vinyl groups were capable of polymerizing with the MMA monomer. At slower polymerization, the nanoparticles self-organized to form a large-length scale network structure with the mass fractal of average dimension of 2.7; contrarily, the nanoparticles exhibited better dispersion when the polymerization proceeded at a faster rate. According to the scenario of perturbed polymerization kinetics in the presence of nanoparticles, we propose a possible mechanism through which the MMA monomers at a lower polymerization rate may constitute longer "multiple grafted PMMA chains" along particle surfaces by an optimal balance between the polymerization of the monomer and the grafting reaction of the monomer onto the particle surface, forming the M-SiO_2-rich clusters by interparticle bridging; the multiple grafting reaction also occurred in between any two neighboring M-SiO_2 nanoparticles situated respectively at the two adjoining clusters to induce the intercluster bridging, thereby leading to a hierarchical fractal network. However, both the polymerization and the grafting reaction of MMA monomers at a higher polymerization rate formed the shorter free and grafted PMMA chains, providing steric stabilization to retain better dispersity of nanoparticles.

1. INTRODUCTION

Inorganic spherical nanoparticles, especially with surface modification of an organic functional shell on the particle surface, have received great attention because of their capability of exhibiting tunable properties.[1−4] The majority of interests involves the use of this type of nanoparticles as nanofiller in a functional polymer matrix to manipulate the inorganic/organic nanocomposite materials with remarkable combined properties for applications in optoelectronic, magnetic, biomimetic, catalytic, and mechanical reinforced fields.[5−11] It has been reported that the intrinsic characteristics of nanoparticles (such as the size[12−19] and concentration[13,14,16] of nanoparticles and the grafting density[13,17,20] and thickness[13,20] of the modified shell) can contribute to the overall properties of the nanoparticle/polymer nanocomposites. To control or enhance their properties toward specific applications, it is of great importance to understand the state of nanoparticle dispersion and the relevant mechanism.[12,15,21−23] So far, much effort has been made both theoretically and experimentally to resolve the nanoparticle dispersion in the polymer matrix;[24−27] nevertheless, well controlling the spatial organization of nanoparticles and understanding the dispersion mechanisms involved are still challenging tasks.

Received: April 19, 2019
Revised: October 9, 2019
Published: October 28, 2019

© 2019 American Chemical Society

DOI: 10.1021/acs.macromol.9b00810
Macromolecules 2019, 52, 8312−8322

The focus of the present study is placed on manipulating the dispersion state of surface-modified nanoparticles in a polymerizing medium to prepare their nanocomposites. The types of surface-modified nanoparticle/polymer nanocomposites can be classified into the following two systems: (1) dressed nanoparticles are surrounded by the polymer matrix without chemical bonding between these two constituents;[28−31] (2) dressed nanoparticles are chemically connected with the polymer matrix, mediated by the establishment of covalent bonding between the surface modifier and the polymer.[32,33] The interesting aspect of the first system is the fine balance between the particle−particle interaction[28−31] and the particle−polymer interaction[28,34,35] to govern the dispersion of nanoparticles after blending with the polymer. Another interesting aspect of the first system is the interplay between the ability of nanoparticles to disperse and the kinetics of polymerization by polymerizing the monomer after prior dispersion of the nanoparticles in the monomer medium; this case was found to often induce particle aggregation for avoiding the conformational entropy loss of matrix chains through the "attractive depletion mechanism".[33] The present study concerns a more complex system, that is, an extension of the second system, involving both the polymerization of the monomer and the grafting reaction of the monomer onto the particle surface through the tethered vinyl groups. In this case, the conformational entropic change of the polymerizing chains is still a critical factor to dominate the chain localization in the interparticle region.[32,33] Moreover, considering that the reactive sites (i.e., the vinyl groups) at the ends of the surface modifiers in this system are designed to be capable of reacting with the monomer, the competition between the polymerization of the monomer and the grafting reaction for polymerization from or to the surface modifiers is another factor that should be considered to examine its impact on the nanoparticle dispersion.

On the other hand, the self-organization of nanoparticles is capable of generating a series of dispersion states depending on the particle concentration, the molecular weight of polymer matrix chains, and the chain length ratio of grafted chains to matrix chains.[23,30,36] Over the dispersion morphologies of nanoparticles reported previously, the fractal network structure exhibiting the self-similarity has recently received much attention owing to the hierarchy of structural features. Two common types of fractal structures have been characterized,[37−40] where one is the fractal aggregates that are formed by the primary nanoparticles are homogenously dispersed inside the matrix without any connectivity, and the other is the aggregates that can be percolated into a continuous network. The latter one may offer attractive potential for developing multifunctional composites based on their hierarchically structural features.

In this study, we reveal that the spherical silica (SiO_2) nanoparticles with surface modified [3-(methacryloyloxy)-propyl]trimethoxysilane (MSMA-modified SiO_2, abbreviated further as M-SiO_2) were successfully dispersed in the methyl methacrylate (MMA) medium for subsequent free radical polymerization to yield the poly(methyl methacrylate)/M-SiO_2 (PMMA/M-SiO_2) nanocomposite. The dispersion state of M-SiO_2 in the PMMA matrix formed by polymerizing the MMA monomer at different initiator concentrations was further investigated to resolve the effect of the polymerization rate on the dispersion behavior of SiO_2 nanoparticles, for which the PMMA chains can be chemically bonded with the nanoparticles through the reaction with the MSMA modifier at the particle surface. It will be shown that, at lower initiator concentration that slowed down the polymerization, M-SiO_2 nanoparticles formed local clusters in which the nanoparticles interacted repulsively and followed by self-organizing the clusters into a fractal structure. In contrast, at higher initiator concentration, where the polymerization was accelerated, M-SiO_2 exhibited much better dispersity than the polymerization proceeded at a lower rate. The observed nanoparticle dispersion behavior will be discussed in connection with the polymerization kinetics of the PMMA matrix. The formation of a polymer nanocomposite with silica nanoparticles through controlling the polymerization kinetics by the different amounts of added initiators offers a convenient approach for inducing a controllable dispersion state of nanoparticles in the nanocomposites. It is noted that the calculation of the polymerization rate can quantitatively reveal its effect on the dispersion of the silica nanoparticles in the PMMA matrix, which was not the interest of the present study.

2. EXPERIMENTAL SECTION

2.1. Materials and Sample Preparation. Aqueous SiO_2 nanoparticles with the particle concentration of 20 wt % (SNOWTEX N20) used here were purchased from Nissan Chemical Industries, Ltd. The SiO_2 nanoparticles were stabilized by the electrostatic repulsion from their negatively charged surfaces induced by the presence of ionic stabilizers (i.e., alkali ions) with counter charge in the solution.

For the surface modification of SiO_2, first, the MSMA silane (which was purchased from Sigma-Aldrich Company, Ltd, with purity up to 98%) was diluted into isopropyl alcohol (IPA) solvent (weight ratio of MSMA/IPA = 1:1) under the ice bath; second, the MSMA solution was further added into the SiO_2 nanoparticle solution under stirring to form a milk white solution; third, the mixed solution was diluted with IPA to form a transparent solution for subsequent reflux at 60 °C for 12 h to obtain the hydrophobic M-SiO_2 nanoparticles. The reflux for M-SiO_2 nanoparticles can significantly improve the surface modification. Upon using the micromixing technique in a high gravity reactor five times, the M-SiO_2 nanoparticles were transferred to the ethyl acetate (EA) for removing the residual alkali ions and nontethered MSMA silanes. Figure S1 of the Supporting Information shows the TGA curve of the resulting M-SiO_2, in which the weight percentage of the tethered MSMA silanes on each SiO_2 nanoparticle was about 27.9 wt %. In addition, the Fourier-transform infrared (FTIR) spectrum of M-SiO_2 nanoparticles is shown in Figure S2 of the Supporting Information, displaying the appearance of 1720, 1635, 1453, 1377, and 1105 cm^{-1} bands for the populations of functional groups in MSMA.[41] Subsequently, the MMA monomer was added to the M-SiO_2/EA solution to prepare the thorough mixed solution of M-SiO_2 and MMA after the complete removal of EA using the rotary evaporator at 45 °C. Because the weight percentage of the MMA monomer in the initial mixed solution of M-SiO_2 and MMA was held at 84.5 wt %, and the MSMA silane and the MMA monomer used here have the equivalent amount of methacrylate groups, the ratio of methacrylate functionalities supplied by grafted MSMA to those of MMA was 0.021 $\left(= \frac{(15.5\text{ wt }\% \times 0.279)\ /\ 248.35}{84.5\text{ wt }\%\ /\ 100.12} \right)$, where 248.35 and 100.12 g/mol were the molecular weights of MSMA and MMA, respectively. Then, the MMA monomer was polymerized using a free radical initiator, azobisisobutyronitrile (AIBN), in bulk process at the prescribed polymerization temperature to yield the PMMA/M-SiO_2 nanocomposites. The weight percentage of the SiO_2 nanoparticles in the nanocomposites was 11.2 wt % (which corresponded to 15.5 wt % M-SiO_2 nanoparticles in the nanocomposites), as determined by the TGA analysis in Figure S3 of the Supporting Information.

2.2. Small-Angle X-ray Scattering Measurement. The dispersion morphology of M-SiO_2 nanoparticles in the MMA medium

DOI: 10.1021/acs.macromol.9b00810
Macromolecules 2019, 52, 8312−8322

and the PMMA matrix was probed by small-angle X-ray scattering (SAXS) performed at the Endstation BL23A1 of the National Synchrotron Radiation Research Center (NSRRC), Taiwan. The energy of the X-ray source and the sample-to-detector distance were 8 keV and 1815 mm, respectively. The scattering signals were collected by using a Pilatus-1MF detector of 981 × 1043 pixel resolution with a typical exposure time of 5 min. Three SAXS measurements were completed on the same piece of each sample for obtaining the intensity profiles with good statistics. The scattering intensity profile was the output as the plot of the scattering intensity (I) versus the magnitude of the scattering vector, $q = (4\pi/\lambda)\sin(\theta/2)$ (θ = scattering angle). The SAXS profiles were corrected for the incident beam intensity, the detector sensitivity, and the background.

The equations used for model fitting in this study are shown as follows[42−51] (the detailed description of the derivations of these equations can be found in the Supporting Information or in the literature[42]).

The polydisperse spherical form factor on the basis of Schultz distribution for the scattering from the primary SiO_2 nanoparticle is given by

$$P(q) = \Delta\rho^2 \langle V_p^2 \Phi^2(q; R_p) \rangle \quad (1)$$

where $\Delta\rho$ is the electron density difference between the SiO_2 nanoparticle and the aqueous solvent, $V_p = \frac{4\pi R_p^3}{3}$ with R_p being the effective radius of the nanoparticle, $\Phi(q;R_p)$ is the amplitude of scattering as a function of q and R_p, and $\langle\ \rangle$ denotes the average with respect to the distribution of R_p.

The polydisperse core−shell spherical form factor on the basis of Schultz distribution for the scattering from the primary M-SiO_2 nanoparticle is given by

$$P(q) = \left\langle \frac{1}{V_{p+s}} \Phi^2(q; R_p, q; R_{p+s}) \right\rangle \quad (2)$$

where $R_{p+s} = R_p + t_s$ with t_s being the MSMA shell thickness and $V_{p+s} = \frac{4\pi R_{p+s}^3}{3}$. The terms associated with the electron density differences between the SiO_2 nanoparticle, the MSMA silane, and the MMA monomer are shown in eq 32 in the Supporting Information.

The hard-sphere potential with the Percus−Yevick (PY) closure or called the hard-sphere model for the scattering from the polydisperse SiO_2 nanoparticles in the PMMA matrix is given by

$$\frac{d\Sigma(q)}{d\Omega} = n\Delta\rho^2 \langle V_p^2 \Phi^2(q; R_p) \rangle S_{ZP}(q; R_{p,av}) \quad (3)$$

where $d\sum(q)/d\Omega$ is the differential scattering cross section for the primary SiO_2 nanoparticles distributed over the infinitely larger PMMA matrix, $n = N/V_{ir}$ with N and V_{ir} being the total number of the SiO_2 nanoparticles in the infinitely large PMMA matrix and the irradiated volume with the incident beam, respectively, and $S_{ZP}(q;R_{p,av})$ is the Zernike−Prins (ZP) structure factor associated with the hard-core repulsive potential for the monodisperse sphere having the average size $R_{p,av}$.

The screened Coulomb potential with the mean spherical approximation closure for the scattering from the polydisperse SiO_2 nanoparticles in aqueous solution is also given by eq 3; however, in this case, $d\sum(q)/d\Omega$ represents the differential scattering cross section for the primary SiO_2 nanoparticles distributed over the infinitely larger aqueous solvent, $n = N/V_{ir}$ with N and V_{ir} being the total number of the SiO_2 nanoparticles in the infinitely large aqueous solvent and the irradiated volume with the incident beam, respectively, and $S_{ZP}(q;R_{p,av})$ is the ZP structure factor associated with the screened Coulomb potential for the monodisperse sphere having the average size $R_{p,av}$.

2.3. Transmission Electron Microscopy (TEM) Observation. The real-space morphology of the dispersion state of M-SiO_2 nanoparticles in the PMMA matrix was observed by using a JEOL JEM-2000 transmission electron microscope (TEM) operated at 120 kV. The ultrathin sections with a thickness of 100 nm were prepared by using a microtome. The ultrathin sections were then picked up onto the copper grids coated with carbon-supporting films. A series of bright-filed micrographs were acquired at tilt angles in the range of ±66° at an angular interval of 1°. The SiO_2 nanoparticles can be served as fiducial markers. The tilt series of the micrographs were then aligned by tracking the fiducial markers, followed by combining all the 2D-aligned micrographs to generate the 3D images. The 3D images were further manipulated to reconstruct the 2D cross-sectional micrographs along the x−y plane of 3D images, where the thickness-setting of a portion in the z direction to be taken for obtaining the cross-sectional images was 45 nm. The SiO_2 nanoparticles appear as the light orange region in the micrograph, while the PMMA matrix corresponds to the deep orange region.

3. RESULTS AND DISCUSSION

3.1. Dispersion of M-SiO_2 Nanoparticles in PMMA/M-SiO_2 Nanocomposite Films. Prior to the surface modification, the aqueous dispersity of the unmodified hydrophilic SiO_2 nanoparticles has been studied. Figure 1 shows the concentration-normalized SAXS profiles of the unmodified SiO_2 nanoparticles in aqueous solution over broad weight percentage ranges. The scattering profiles of both 0.1 and 1.0 wt % showed a Guinier region in the low-q profile followed by a q^{-4} power law dependence of the scattering intensities in the high-q region. Such asymptotic scattering behavior indicates that the SiO_2 nanoparticles were spherical in shape and were dispersed without apparent interaction. The red solid curve represents the fit of the scattering profile of 0.1 wt % by the polydisperse spherical form factor, yielding unmodified SiO_2 ($\bar{R}_{SiO_2}$) of a mean radius of 7.05 nm ± 0.006. When the particle concentration was increased to 10 wt %, an interaction peak appeared at 0.018 $Å^{-1}$ in the low-q region. This interaction peak was characteristic to the hard-sphere interaction under the high content of nanoparticles or the electrostatic repulsion between the nanoparticles as they were charged. In the latter case, the surface charge yielded an electrical double layer to stabilize the SiO_2 dispersion. The interaction peak sharpened and the peak position shifted to higher q at 0.023 $Å^{-1}$ upon further increasing the particle concentration to 15.5 wt %,

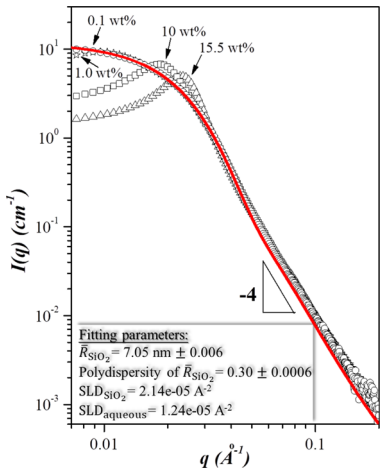

Figure 1. Concentration-normalized SAXS profiles of the unmodified SiO_2 nanoparticles dispersed in the aqueous solution at different weight percentages ranging from 0.1 to 15.5 wt %. Red solid curve represents the fit of the experimental data by the spherical form factor with radius distribution. Inset shows the key parameters to fit the data.

DOI: 10.1021/acs.macromol.9b00810
Macromolecules 2019, 52, 8312−8322

indicating the much stronger hard-sphere interaction at a shorter interparticle distance or the stronger electrostatic repulsion. The fact that the SAXS profiles obtained at the lower concentrations can be fitted well by the spherical form factor, and the presence of the repulsive interaction peak at the higher concentrations reveals that the unmodified hydrophilic SiO_2 nanoparticles were dispersed well in the aqueous medium.

However, when the aqueous dispersion of the unmodified SiO_2 nanoparticles was transferred to the organic MMA monomer, precipitation occurred because of the aggregation of the nanoparticles with the hydrophilic surface. To achieve good dispersion of the SiO_2 nanoparticles in the organic MMA medium, we modified the particle surface by MSMA silane to not only enhance the solubility with the MMA monomer but also introduce the steric stabilization even at a high particle content. Figure 2 shows the SAXS profile of M-SiO_2 dispersion

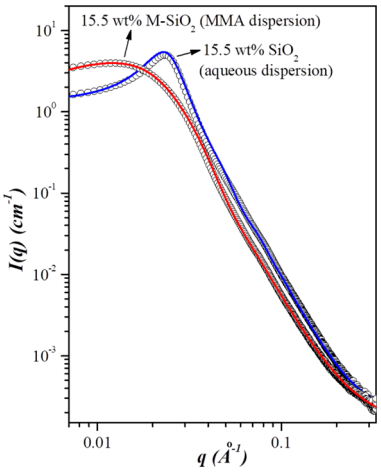

Figure 2. SAXS profiles of the M-SiO_2 nanoparticles dispersed in the MMA monomer and the unmodified SiO_2 nanoparticles dispersed in the aqueous solution at the same particle concentration of 15.5 wt %. Red and blue solid curves represent the fits of the experimental data by the polydisperse core−shell spherical form factor and the polydisperse spherical form factor with the screened Coulomb potential, respectively.

in the MMA monomer (concentration = 15.5 wt %) along with that of unmodified SiO_2 in aqueous solution, and the fit of the scattering profiles of the polydisperse core−shell spherical form factor and the polydisperse spherical form factor with the screened Coulomb potential to the experimental data of MMA and aqueous dispersion, respectively, are also displayed in Figure 2. The key parameters yielded by model fitting are summarized in Table 1. It can be seen that the surface modification by silane groups significantly improved the dispersity of SiO_2 nanoparticles in the MMA monomer, as characterized by the disappearance of the repulsive interaction peak that has initially appeared in the SAXS profile of the aqueous dispersion of unmodified SiO_2. In the case of aqueous dispersion, the surface charge of SiO_2 obtained by model fitting was found to be ca. −194 mV, which corresponded to the general aqueous dispersion behavior of nanoparticles displaying good stability.[52] While in the case of MMA dispersion, the stabilization mechanism was replaced by the steric repulsion between the silane groups at particle surfaces, where the thickness of the silane shell accounted for at least 7.1% of the overall radius of the M-SiO_2 nanoparticle, as calculated by the

Table 1. Key Parameters Yielded by Model Fitting of the SAXS Profiles in Figure 2, Where $\bar{t}_{MSMA}$ is the Mean Thickness of the Modified MSMA Shell and SLD_i Represents the Scattering Length Densities of the Different Components *i*

	vol %[a]	$\bar{R}_{SiO_2}$ (nm)	polydispersity of $\bar{R}_{SiO_2}$	$\bar{t}_{MSMA}$ (Å)	surface charge (mV)	SLD_{SiO_2} ($Å^{-2}$)	SLD_{MSMA} ($Å^{-2}$)	SLD_{medium}[b] ($Å^{-2}$)
M-SiO_2 in MMA medium	7.03	7.05 ± 0.006	0.30 ± 0.0006	5.4 ± 1.2		2.14×10^{-5}	$2.06 \times 10^{-5} \pm 3.19 \times 10^{-9}$	$2.08 \times 10^{-5} \pm 6.49 \times 10^{-10}$
SiO_2 in aqueous medium	6.83	7.05 ± 0.006	0.30 ± 0.0006		−193.95 ± 0.85	2.14×10^{-5}		$2.07 \times 10^{-5} \pm 4.79 \times 10^{-10}$

[a]Volume fractions (vol %) of 7.03 and 6.83 for M-SiO_2 and SiO_2 nanoparticles, respectively, were fixed in the fitting procedure, both of which corresponded to 15.5 wt % when using the SiO_2, MSMA, MMA medium, and aqueous medium of specific densities of 2.5, 1.045, 0.94, and 1 g/cm^3, respectively, for the conversion of units. [b]Deviation of SLD for the aqueous medium from water was probably because of the presence of the alkali ions in the aqueous medium.

DOI: 10.1021/acs.macromol.9b00810
Macromolecules 2019, 52, 8312−8322

fitted values of $\bar{R}_{SiO_2}$ and the MSMA shell thickness ($\bar{t}_{MSMA}$). The grafting density (=ca. 1.5 chains/nm^2) of MSMA silanes on the particle surface can further be estimated by $\frac{\left\{\frac{4\times\pi}{3}\times[((\bar{R}_{SiO_2}+\bar{t}_{MSMA})\times10^{-7})^3-(\bar{R}_{SiO_2}\times10^{-7})^3]\right\}\times1.045\ \mathrm{g/cm^3}\times\frac{N_A}{MW_{MSMA}}}{4\times\pi\times\bar{R}_{SiO_2}{}^2}$, with MW_{MSMA} and N_A being the molecular weight of MSMA (=248.35 g/mol) and the Avogadro number (=6.02 × 10^{23}), respectively. The interaction between M-SiO_2 nanoparticles was describable by the hard-sphere interaction, which was essentially a repulsive interaction. This demonstrated that M-SiO_2 nanoparticles with good dispersity in the MMA monomer have been successfully prepared by the surface modification, and the polymer nanocomposites can be prepared by polymerization of the MMA monomer with the reduction in possibility of inducing particle aggregation.

The mixture through thorough mixing of M-SiO_2 nanoparticles, the MMA monomer, and the AIBN initiator was used as the precursor solution to prepare PMMA/M-SiO_2 nanocomposites. It is noted that the tethered MSMA silanes bearing vinyl groups also served as the reactive sites for the MMA monomer to undergo addition polymerization. Figure 3 shows

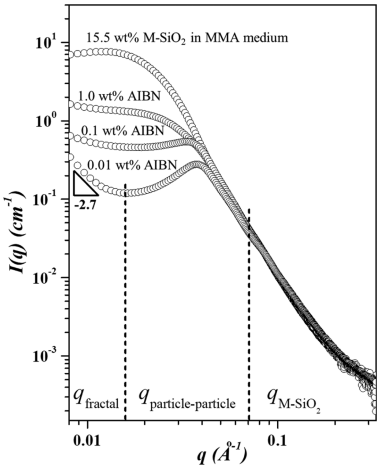

Figure 3. SAXS profiles of the PMMA/M-SiO_2 nanocomposites collected after the precursor solutions, that is, 15.5 wt % M-SiO_2 dispersed in the MMA medium with different amounts of AIBN initiator (=0.01, 0.1, and 1.0 wt %), have been prepolymerized at 75 °C for 3 h followed by polymerization at 100 °C for 3 h.

the SAXS profiles of the PMMA/M-SiO_2 nanocomposites collected after the precursor solutions (i.e., 15.5 wt % M-SiO_2 dispersed in the MMA monomer with different amounts of the AIBN initiator) have been prepolymerized at 75 °C for 3 h followed by polymerization at 100 °C for 3 h. For the composite polymerized at 0.01 wt % AIBN, an interaction peak at q = 0.038 Å^{-1} was observed along with an intensity upturn at q < 0.016 Å^{-1} in the low-q region. Because such an interaction peak was absent in the scattering profile of the precursor solution, in which M-SiO_2 nanoparticles displayed the independent scattering feature of the uniform dispersion (see Figure 2), it means that domains containing higher concentration (than the overall concentration, i.e., 15.5 wt %) of nanoparticles were formed upon polymerization. In this case, the interaction peak was associated with the nanoparticles interacting via repulsive hard-sphere potential within the cluster domains under a higher particle content. The intensity upturn displaying a $q^{-2.7}$ power law dependence of scattering intensities in the low-q region may further indicate the formation of a large-length scale network structure with a mass fractal of average dimension of 2.7 (the complemented SAXS profile covering more low-q data points is shown in Figure S4 of the Supporting Information to investigate the feature of power law exponent of mass fractal). With the increase of the initiator concentration, the interaction peak became smeared at 0.1 wt % AIBN and eventually disappeared at 1.0 wt % AIBN, clearly demonstrating that the phase separation that generated the particle-rich cluster domains was suppressed by increasing initiator concentration; nevertheless, the intensity upturn was still observable but with the exponents of power law (i.e., −0.9 and −0.4 for 0.1 and 1.0 wt % AIBN, respectively) lower than that expected for the fractal network. Namely, the M-SiO_2-rich domains still formed but the structural feature was not as compact as that of the fractal structure because the particle concentration in the domains was lower. The SAXS study shown here may reveal how the polymerization kinetics of PMMA affected the dispersion state of M-SiO_2 nanoparticles as the fact that increasing the initiator concentration can speed up the rate of free radical polymerization of PMMA and vice versa.[53]

Besides the initiator concentration, increasing the polymerization temperature was also able to speed up the reaction; therefore, a similar trend was found in Figure S5 of the Supporting Information, which shows the SAXS profiles of the PMMA/M-SiO_2 nanocomposites collected after the precursor solution (i.e., 15.5 wt % M-SiO_2 dispersed in the MMA medium with 0.1 wt % AIBN) has been, respectively, prepolymerized at different prescribed temperatures (=65, 75, and 85 °C) for 3 h followed by polymerization at 100 °C for 3 h. It is thus suggested that controlling the polymerization rate by both initiator concentration and reaction temperature offers an efficient way of tailoring the dispersion state of M-SiO_2 nanoparticles in the PMMA/M-SiO_2 nanocomposite system.

To complement the SAXS study, the nanocomposites were cut into ultrathin sections for the real-space observation. The 3D electron tomography of the nanocomposite film prepared at 0.01 wt % AIBN is shown in Figure S6a of the Supporting Information. Because the projections of the cluster domains in the ultrathin section may have superimposed extremely under the high particle concentration, the 3D image in Figure S6a was further manipulated to reconstruct the 2D cross-sectional micrograph along the $x-y$ plane of the 3D image, where the thickness-setting of the portion in the z direction to be taken for obtaining the cross-sectional image was 45 nm; in this situation, the maximum number of primary M-SiO_2 nanoparticles distributed in the z-depth of the portion that could generate overlapped 2D projections were three particles at most. The reconstructed 2D micrograph is shown in Figure 4a, which represents the real-space evidence of the fractal network structure featuring the connectivity of M-SiO_2 nanoparticles. As for the nanocomposite prepared at 1.0 wt % AIBN, it can be seen from the 3D tomography (see Figure S6b) or its reconstructed 2D image (see Figure 4b) that the observation of the dispersed morphology of nanoparticles was consistent with that studied by SAXS.

Our SAXS and TEM results have revealed that the dispersion state of M-SiO_2 nanoparticles was significantly dependent on the polymerization rate of the PMMA matrix, primarily controlled by the initiator concentration or the polymerization temperature; particularly, in the case of the

DOI: 10.1021/acs.macromol.9b00810
Macromolecules 2019, 52, 8312−8322

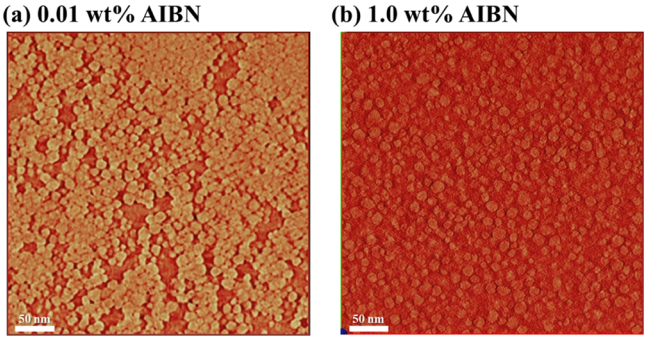

Figure 4. Two-dimensional cross-sectional micrographs of the nanoparticle dispersion in the PMMA/M-SiO_2 nanocomposites prepared at (a) 0.01 wt % AIBN and (b) 1.0 wt % AIBN, respectively, which were reconstructed from the 3D TEM images shown in Figure S6 of the Supporting Information. SiO_2 nanoparticles appear as the light orange region in the micrograph, while PMMA matrix corresponds to the deep orange region.

lower polymerization rate, the self-organization of M-SiO_2 nanoparticles exhibited two characteristic levels of the structure. The first level was the M-SiO_2-rich cluster domains, in which the particle concentration was higher than the overall particle concentration; the second level was associated with the mass fractal structure constructed by clusters showing the average dimension of 2.7. Contrarily, the nanocomposite prepared at the higher polymerization rate was characterized by the formation of relatively dispersed morphology of M-SiO_2 nanoparticles instead of the compact clusters.

The dependence of nanoparticle dispersion on the polymerization rate of PMMA can be traced to its correlation with the resultant molecular weight of the PMMA matrix. Some relevant studies have focused on the composite systems with the bare nanoparticles or the polymer-grafted nanoparticles, which were simply hybridized by the polymer matrix without forming covalent bonds between them.[22,23,30,36] Akcora et al. reported the formation of spherical aggregates, interconnected network, short strings, and dispersed nanoparticles sequentially in the polystyrene-grafted SiO_2/polystyrene nanocomposites with increasing the ratio of the chain length of grafted polystyrene to matrix polystyrene at fixed particle loading of 5 wt %.[30] They further observed a similar trend in the PMMA-grafted SiO_2/PMMA nanocomposites but with a higher particle concentration of 15 wt %, showing that at the lower and the higher chain length ratios of grafted PMMA to matrix PMMA resulted the nanoparticle agglomerates and the well-dispersed nanoparticles, respectively.[23] The particle dispersity in these two composite systems, in which both grafted and matrix chains were chemically identical, was suggested to rely on the miscibility between the two parts of chains essentially obeying the autophobic dewetting behavior.[23,34] In comparison to the polymer-grafted nanoparticles, the dispersion behavior of bare nanoparticles became different as can be found in the SiO_2/poly(ethyl methacrylate) nanocomposites by Banc et al.,[36] which reported that the slowed-down kinetics of the spatial reorganization of SiO_2 nanoparticles caused by the higher molecular weight of the matrix (160 kg/mol) led to the individual dispersion, whereas the lower molecular weight (20 kg/mol) favored the formation of small aggregates over a wide range of particle concentration from 2 to 18 wt %.

To understand the influence of the matrix molecular weight in the PMMA/M-SiO_2 nanocomposites, a complete removal of SiO_2 nanoparticles is necessary but it may lead to the chain scission of the matrix resulting in chains, which are of lower molecular weight than expected. It has been reported that the free radical polymerization of PMMA in the presence of modified silica nanoparticles with reactive vinyl groups could still obey the steady state and pseudo-first order kinetics; furthermore, the modification caused an increase in reaction rate and conversion, while it did not change the kinetic behavior of polymerization.[54] Therefore, we intended to evaluate the molecular weight of the PMMA matrix through measuring the corresponding neat PMMA homopolymer constituted under the same polymerization conditions as were nanocomposites. The gel permeation chromatography (GPC) elution curves of the neat PMMA samples prepared with the addition of 0.01, 0.1, and 1.0 wt % AIBN are shown in Figure S7 of the Supporting Information. Indeed, decreasing the AIBN concentration by hundred times from 1.0 to 0.01 wt % can substantially increase the molecular weight of PMMA. Although the molecular weights were not directly measured from the PMMA component of the nanocomposites, the GPC study could still reveal the importance of matrix chain size in tailoring the state of nanoparticle dispersion in the PMMA/M-SiO_2 nanocomposites, considering the dominant role of initiator concentration in determining the chain length of PMMA even in the presence of nanoparticles.[54]

3.2. Proposed Mechanism of M-SiO_2 Dispersion in PMMA/M-SiO_2 Nanocomposite Films. The particle concentration (=15.5 wt %) in our PMMA/M-SiO_2 nanocomposite system is comparable with that (=18 wt %) studied by Banc et al.;[36] however, we present a contrary result revealing that the formation of cluster domains with the crowded arrangement of nanoparticles was favored as the PMMA chains were allowed to grow with higher molecular weights at a lower polymerization rate. It has been reported by the attractive depletion mechanism that the particle aggregation in a polymerizing medium was an entropic nature associated with the expellant of growing polymer chains from the interparticle region to avoid the conformational entropy loss;[33] this mechanism was essentially proposed under the condition of without the occurrence of chemical reaction (e.g., grafting reaction) at the particle surface. In contrast, in the present PMMA/M-SiO_2 nanocomposite system, the vinyl groups of the tethered silanes located at the SiO_2 surface can participate in the polymerization with the MMA monomer. As a result, we may envision the following possible factor (against the slowed-down kinetics[36]) to "pull" nanoparticles close to each other to form the clusters at a slower polymerization rate with the growth of longer PMMA chains: a chemical factor involving the bridging of PMMA chains on nanoparticles via the polymerization of the monomer accompanying with the grafting reaction of the monomer onto the particle surface through the tethered vinyl groups. We propose that the bridging effect on the formation of clusters may cause entropic penalty arising from the translational entropy loss on binding of polymer chains to particle surfaces and thus induce a strong repulsive interaction between nanoparticles. Below, we will first discuss the repulsive interaction observed by SAXS and then the possible mechanism of bridging.

As revealed in Figure 3, the repulsive interaction was characterized by the SAXS pattern of 0.01 wt % AIBN showing a strong interaction peak at q = 0.038 $Å^{-1}$. This SAXS profile was basically collected at the temperature (=25 °C) much lower than the glass transition temperature of the PMMA

DOI: 10.1021/acs.macromol.9b00810
Macromolecules 2019, 52, 8312−8322

chains ($T_g^{PMMA} \cong 105$ °C); intuitively, it seems to be practicable to smear out the peak intensity of such an interaction peak by increasing the chain mobility in the PMMA matrix at an elevated temperature to gain more translational entropy. However, this scenario did not happen as expected; instead, the peak intensity was found to persist even on heating the sample to 160 °C, as revealed by the red circle curve in Figure 5. The obvious change of the scattering feature on

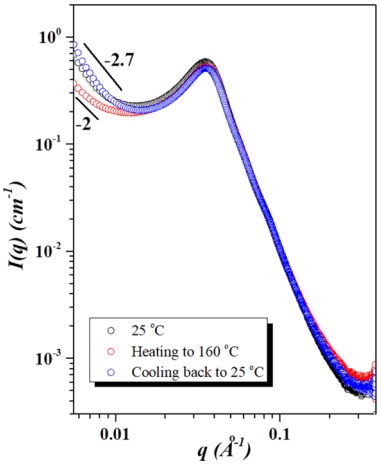

Figure 5. Black circle curve: SAXS profile collected at 25 °C of the fractal-forming PMMA/M-SiO_2 nanocomposite (i.e., the same trace as that for the nanocomposite prepared at 0.01 wt % AIBN in Figure 3); red circle curve: SAXS profile of the same nanocomposite collected at 160 °C after annealing at 160 °C for 20 min; blue circle curve: SAXS profile of the same nanocomposite collected at 25 °C again after a subsequent cooling from 160 to 25 °C.

heating was only a limited reduction in the upturned intensity at $q < 0.016$ Å^{-1}, probably associated with a slight perturbation of the fractal structure as indicated by the decrease of the slope of power law from −2.7 (shown in the black circle curve) to −2 (shown in the red circle curve). Nevertheless, the low-q scattering profile was recovered to the level as the initial one with the $q^{-2.7}$ power law upon subsequently cooling the sample back to 25 °C, as displayed by the blue circle curve. This temperature-dependent experiment shows that the entropy-induced repulsive interaction between nanoparticles within the cluster domains cannot be disrupted by the thermal effect, thus implying that the PMMA chains have been strongly constrained in the interparticle region through grafting with the tethered silanes. It is noted that one would also expect that the structure associated with interparticle arrangement evolves toward a more aggregated state upon annealing leading to a stronger interaction peak, which was however not observed in the present study.

To elucidate the nanoparticle dispersion within each cluster by studying the repulsive interaction peak, the model fitting by the PY structure factor considering the hard-sphere potential was applied to fit the repulsive interaction peak, as shown in Figure 6, yielding an effective radius of 7.6 nm along with an effective volume fraction of 26 vol % (the fitting results of the SAXS patterns of 0.1 and 1.0 wt % AIBN are shown in Figure S8 of the Supporting Information). The obtained parameters represent that the nanoparticles within each cluster interacted repulsively by a distance of 15.2 nm (i.e., double the effective radius and was larger than the interparticle distance of direct contact), for which the corresponding volume fraction of the

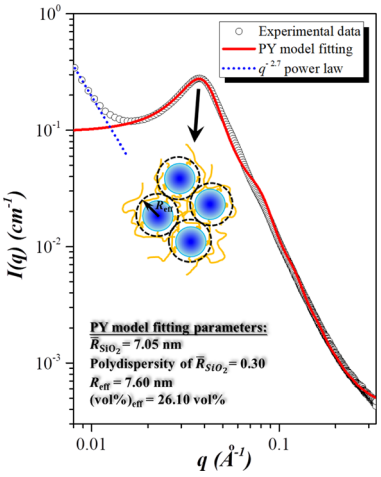

Figure 6. Fit of the SAXS profile of the PMMA/M-SiO_2 nanocomposite prepared at 0.01 wt % AIBN by the PY structure factor (the red solid curve) to resolve the repulsive interaction peak associated with the hard-sphere potential between M-SiO_2 nanoparticles within the cluster. $q^{-2.7}$ power law dependence of the scattering intensities in the low-q region is represented by the blue dashed line. Inset illustrates the nanoparticles interacted repulsively with the hard-sphere interaction by an effective radius, R_{eff}, for which the effective volume fraction (vol %)$_{eff}$ of the entities with R_{eff} (as contoured by the black-dashed circles) was 26.1 vol %.

entities with 7.6 nm in radius (as contoured by the black dashed circles) within each cluster was 26.1 vol %, as schematically illustrated in the inset of Figure 6. This scenario illustrates a certain amount of PMMA chains constituting the corona (with ca. 5.5 Å in thickness) around each M-SiO_2 nanoparticle behaved as an effective part of the entity to induce the hard-sphere interaction. It was however found that the thickness of the PMMA corona corresponded to that of the neat MSMA shell (=ca. 5.4 Å). While considering the situation of the low grafting density of MSMA silanes (=ca. 1.5 chains/nm^2), which may indicate that the particle surfaces of silica nanoparticles would probably still have enough space for the bridging PMMA chains to occupy by intimately wrapping around the nanoparticles along their surfaces during polymerization; in this case, the PMMA chains and the silanes were able to jointly constitute the corona with a thickness corresponding to that of the neat silane shell. Furthermore, the value of 26.1 vol % was quite higher than the overall particle concentration (=7.03 vol %, calculated from the value of 15.5 wt % using the specific densities of 2.5 and 0.94 g/cm^3 for SiO_2 and PMMA, respectively), certainly indicating that the bridging of M-SiO_2 particles through longer PMMA chains has effectively induced a phase separation, which gave rise to the M-SiO_2-rich cluster domains. It is noted that the effective radius obtained for the higher AIBN concentration at 0.1 wt % was the same as that for 0.01 wt % AIBN but with a lower effective volume fraction of 18.5 vol %, implying the formation of M-SiO_2-rich domains containing the lower effective entity concentration to form the loose structure in each cluster. Such structural change in the packing type of the M-SiO_2-rich cluster with increasing AIBN concentration led to a significant reduction in the exponent of power law in the low-q region, as shown in Figure S8 (i.e., the decrease of the slope from −2.7 to −0.9). However, the PY structure factor was invalid to fit the SAXS profile of 1.0 wt % AIBN because of the absence of the

DOI: 10.1021/acs.macromol.9b00810
Macromolecules 2019, 52, 8312−8322

interaction peak; in this case, the exponent of power law in the low-q region was decreased to −0.4.

Hooper and Schweizer have developed a microscopic polymer reference interaction site model (PRISM) to study the potential of mean force between a pair of spherical particles dissolved in an adsorbing homopolymer melt;[55] moreover, they built on the prior work to treat a key thermodynamic property (i.e., particle second virial coefficient) to investigate the spinodal demixing in polymer nanocomposites composed of flexible chains and spherical nanoparticles.[56] Upon their computational study using PRISM at the highest values of the monomer−particle interfacial strength at contact investigated, two distinct phase separation behaviors involving the local bridging of particles by polymers were predicted, where the longest-range tele-bridging attraction (which exhibited distinct adsorbed layers coexisted with longer-range bridging) was stronger than the shorter-range segment-level tight particle bridging attraction.[55,56] Although our proposed chemistry-related particle bridging by the longer PMMA chains in the PMMA/M-SiO_2 nanocomposite system was plausibly similar to the case of telebridging because there was a nonignored size of the PMMA corona part around each M-SiO_2 (∼7.7 Å in thickness), it should be noted that the factor of chemistry-related bridging has not been considered in the previous PRISM computational study.

Let us now consider the possible mechanism of the particle bridging in PMMA/M-SiO_2 nanocomposites via dealing with the polymerization kinetics of PMMA. It is known that the rate of free radical polymerization can be represented by the rate at which the addition of monomers to the growing chains, namely, the rate of propagation (R_p);[57,58] furthermore, on the assumption that the polymerization is performed with a hemolysis initiation under the steady-state condition,[59,60] the rate of propagation is given by $R_p = k[M][I]^{1/2}f^{1/2}$, where $k = k_p\left(\frac{k_d}{k_t}\right)^{1/2}$ with k_p, k_d, and k_t being the rate constants of chain propagation, hemolysis initiation, and overall termination, respectively, [M] is the monomer concentration, [I] is the initiator concentration, and f is called the initiator efficiency, which refers to the fraction of radicals generated by the hemolysis that initiates the chain growth. The previous study has also reported that free radicals can be attached to particle surfaces, which lowered their mobility and hence, the propagation rate;[54] consequently, the term f in the equation based on the free radical polymerization of PMMA in the presence of M-SiO_2 nanoparticles can be modified as f' considering both the effects of the initiator efficiency and the reduced mobility of radicals by nanoparticles. Therefore, the rate of PMMA polymerization in the nanocomposites can be written as

$$R_p = k[\mathrm{MMA}][\mathrm{AIBN}]^{1/2}f'^{1/2} \tag{4}$$

Similarly, the kinetic chain length (ν) defined as the average length of the growing polymer chains[57] in the PMMA/M-SiO_2 nanocomposite system can be expressed as

$$\nu = k'[\mathrm{MMA}][\mathrm{AIBN}]^{-1/2}f'^{-1/2} \tag{5}$$

where $k' = \frac{k_p}{2(k_dk_t)^{1/2}}$. Because we have fixed the concentration of the MMA monomer over the preparation of the nanocomposites, the term of [AIBN] in the right-hand side of eqs 4 and 5 became important in controlling both the rate of polymerization and the kinetic chain length. In this study, with varying [AIBN] from 0.01 to 1.0 wt %, it may cause an increase in R_p by ten times, while giving rise to a reduction in ν by ten times.

According to the general relationship between [AIBN], R_p, and ν, we propose that, at the lower polymerization rate by the addition of AIBN concentration ≤0.01 wt %, the vinyl groups of the tethered silanes on the SiO_2 surface could react with the MMA monomer to constitute the long grafted PMMA chains that thus locally bridged the neighboring nanoparticles. If the grafting reaction was primarily facilitated by means of anchoring the polymerizing PMMA chains to the SiO_2 surface through tethered silanes (i.e., by the "grafting-to" mode), the demixing between SiO_2 nanoparticles and polymerizing PMMA chains should have took place to greatly induce particle aggregation via the attractive depletion mechanism prior to the occurrence of the chain grafting. However, we can rule out this possibility of "grafting-to" reaction evidently from the experimentally observed fractal network structure rather than forming the isolated particle aggregates without connectivity in this study. Thus, we can focus on the issue whether the particle bridging would lead to the formation of cluster domains and followed by the self-organization of clusters into the fractal network.

As mentioned that the propagation rate of chain growing in the presence of nanoparticles would become lowered because of the reduced mobility of free radicals by the particle surface;[54] therefore, when applying this concept to the PMMA/M-SiO_2 nanocomposites and further considering only 0.01 wt % AIBN was added, the situation of propagation rate decreasing may become severe. Thus, we propose that, as schematically illustrated in Figure 7a, MMA monomers at a lower initiator concentration have enough time to constitute longer "multiple grafted PMMA chains" (as presented in green color) along the particle surfaces by an optimal balance between the rates of the polymerization of the monomer and the grafting reaction of the monomer onto the particle surface, where half the ends of the PMMA chains are grafted to a number of SiO_2 nanoparticles and the other ends are anchored to the neighboring nanoparticles, thereby intimately bridging (and probably coupled with some extent of wrapping around) the SiO_2 nanoparticles. This kind of interparticle bridging effect can induce phase separation to form the M-SiO_2-rich cluster domains. Additionally, the multiple grafting reaction can also take place in between any two neighboring M-SiO_2 nanoparticles situated, respectively, at two adjoining clusters to bring about the intercluster bridging (as presented by the chains in red color) for constructing a hierarchical structure of the mass fractal network with the average dimension of 2.7. On the other hand, a portion of longer free PMMA chains (as presented in orange color) can be formed and localized in the interparticle region.

In the case of the higher polymerization rate with the addition of AIBN concentration ≥1.0 wt %, both polymerization and grafting reaction could just allow the monomer to grow into the shorter free and grafted PMMA chains; in this case, the grafted PMMA chains cannot bridge the nanoparticles because of their limited chain length, as schematically illustrated in Figure 7b. However, the coexistence of the free and grafted PMMA chains with shorter chain size may provide steric stabilization to retain the better dispersion morphology.

DOI: 10.1021/acs.macromol.9b00810
Macromolecules 2019, 52, 8312−8322

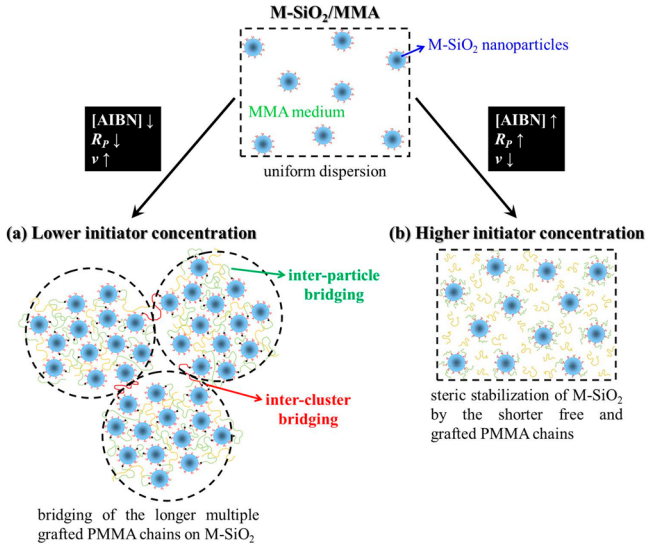

Figure 7. Schematic illustration of the possible mechanism of nanoparticle dispersion in PMMA/M-SiO_2 nanocomposites. (a) At lower AIBN concentration (≤0.01 wt %), the participation of the tethered silanes in the polymerization with the MMA monomer could take place effectively to form the "multiple grafted PMMA chains" (as presented in green color), thus locally bridging the neighboring nanoparticles; this interparticle bridging led to the formation of clusters. Besides, the multiple grafting reaction may also occur in between any two neighboring nanoparticles situated, respectively, at two adjoining clusters to form the intercluster bridging (as presented by the chains in red color). Meanwhile, free PMMA chains could also be formed during the polymerization, as displayed by the chains in orange color. (b) At higher AIBN concentration (≥1.0 wt %), the nanoparticles were dispersed by the steric stabilization from the coexistence of the free and grafted PMMA chains with limited chain length.

4. CONCLUSIONS

The dependence of the dispersion state of M-SiO_2 nanoparticles on the polymerization rate of the PMMA matrix in PMMA/M-SiO_2 nanocomposites has been revealed in this study. At slower polymerization by the addition of initiator at lower concentration, the mass fractal network with the average dimension of 2.7 was formed by the self-organization of nanoparticle clusters in which the M-SiO_2 nanoparticles were packed densely. When the polymerization proceeded at a faster rate at higher initiator concentration, the particles formed another type of clusters in which the nanoparticles were relatively dispersed. A kinetic mechanism of the formation of the fractal structure was deduced through the perturbed polymerization kinetics of the PMMA matrix. We proposed that MMA monomers at lower initiator concentration may constitute longer "multiple grafted PMMA chains" along particle surfaces, thereby intimately bridging M-SiO_2 nanoparticles by the interparticle bridging effect and probably coupled with some extent of wrapping around nanoparticles to form the M-SiO_2-rich cluster domains. The multiple grafting reaction may also take place in between any two neighboring M-SiO_2 nanoparticles situated, respectively, at two adjoining clusters to bring about the intercluster bridging, constructing a fractal network structure. While at the higher initiator concentration, both polymerization and grafting reaction favored the growth of shorter free and grafted PMMA chains, providing steric stabilization to retain the better dispersity of nanoparticles.

■ ASSOCIATED CONTENT

Supporting Information

The Supporting Information is available free of charge on the ACS Publications website at DOI: 10.1021/acs.macromol.9b00810.

Description of the derivations of equations used for model fitting in this study; TGA curve of M-SiO_2 nanoparticles; FTIR spectrum of M-SiO_2 nanoparticles; TGA curve of PMMA/M-SiO_2 nanocomposites; SAXS profile with minimum q down to 0.0024 $Å^{-1}$ of PMMA/M-SiO_2 nanocomposites; SAXS profiles of PMMA/M-SiO_2 nanocomposites prepared at different polymerization temperatures; 3D TEM images of PMMA/M-SiO_2 nanocomposites prepared at different AIBN concentrations; GPC curves of neat PMMA polymerized at different AIBN concentrations; fits of SAXS profiles of PMMA/M-SiO_2 nanocomposites prepared at different AIBN concentrations (PDF)

■ AUTHOR INFORMATION

Corresponding Author

*E-mail: cychu0123@dragon.nchu.edu.tw.

ORCID

Che-Yi Chu: 0000-0002-8482-903X

Ying-Chih Pu: 0000-0003-0685-7200

Notes

The authors declare no competing financial interest.

■ ACKNOWLEDGMENTS

This work is supported by the Ministry of Science and Technology (MOST) Taiwan under grant no. MOST 106-2218-E-005-022-MY2.

■ REFERENCES

(1) Maliakal, A.; Katz, H.; Cotts, P. M.; Subramoney, S.; Mirau, P. Inorganic Oxide Core, Polymer Shell Nanocomposite as a HighKGate Dielectric for Flexible Electronics Applications. *J. Am. Chem. Soc.* **2005**, *127*, 14655−14662.

(2) Guo, Z.-S.; Zhao, L.; Pei, J.; Zhou, Z.-L.; Gibson, G.; Brug, J.; Lam, S.; Mao, S. S. CdSe/ZnS Nanoparticle Composites with Amine-Functionalized Polyfluorene Derivatives for Polymeric Light-Emitting Diodes: Synthesis, Photophysical Properties, and the Electroluminescent Performance. *Macromolecules* **2010**, *43*, 1860−1866.

(3) Gupta, A. K.; Gupta, M. Synthesis and Surface Engineering of Iron Oxide Nanoparticles for Biomedical Applications. *Biomaterials* **2005**, *26*, 3995−4021.

(4) Ripika, P. New Directions in Fluxgate Sensors. *J. Magn. Magn. Mater.* **2000**, *215*−*216*, 735−739.

(5) Nguyen, T.-P. Polymer-Based Nanocomposites for Organic Optoelectronic Devices. A Review. *Surf. Coat. Technol.* **2011**, *206*, 742−752.

(6) Li, S.; Meng Lin, M.; Toprak, M. S.; Kim, D. K.; Muhammed, M. Nanocomposites of Polymer and Inorganic Nanoparticles for Optical and Magnetic Applications. *Nano Rev.* **2010**, *1*, 5214−5233.

(7) Hanemann, T.; Szabó, D. V. Polymer-Nanoparticle Composites: From Synthesis to Modern Applications. *Materials* **2010**, *3*, 3468−3517.

(8) Lapidot, S.; Meirovitch, S.; Sharon, S.; Heyman, A.; Kaplan, D. L.; Shoseyov, O. Clues for Biomimetics from Natural Composite Materials. *Nanomedicine* **2012**, *7*, 1409−1423.

(9) Ramakrishna, S.; Mayer, J.; Wintermantel, E.; Leong, K. W. Biomedical Applications of Polymer-Composite Materials: A Review. *Compos. Sci. Technol.* **2001**, *61*, 1189−1224.

DOI: 10.1021/acs.macromol.9b00810
Macromolecules 2019, 52, 8312−8322

(10) Sanchez, C.; Julián, B.; Belleville, P.; Popall, M. Applications of Hybrid Organic-Inorganic Nanocomposites. *J. Mater. Chem.* **2005**, *15*, 3559−3592.
(11) Chen, Q.; Gong, S.; Moll, J.; Zhao, D.; Kumar, S. K.; Colby, R. H. Mechanical Reinforcement of Polymer Nanocomposites from Percolation of a Nanoparticle Network. *ACS Macro Lett.* **2015**, *4*, 398−402.
(12) Yang, W.; Yi, R.; Yang, X.; Xu, M.; Hui, S.; Cao, X. Effect of Particle Size and Dispersion on Dielectric Properties in ZnO/Epoxy Resin Composites. *Trans. Electr. Electron. Mater.* **2012**, *13*, 116−120.
(13) Oh, H.; Green, P. F. Polymer Chain Dynamics and Glass Transition in Athermal Polymer/Nanoparticle Mixtures. *Nat. Mater.* **2009**, *8*, 139−143.
(14) Zhang, S.; Cao, X. Y.; Ma, Y. M.; Ke, Y. C.; Zhang, J. K.; Wang, F. S. The Effects of Particle Size and Content on the Thermal Conductivity and Mechanical Properties of Al_2O_3/High Density Polyethylene (HDPE) Composites. *eXPRESS Polym. Lett.* **2011**, *5*, 581−590.
(15) Li, X.; Park, W.; Chen, Y. P.; Ruan, X. Effect of Particle Size and Aggregation on Thermal Conductivity of Metal-Polymer Nanocomposite. *J. Heat Transfer* **2017**, *139*, 022401.
(16) Kutvonen, A.; Rossi, G.; Puisto, S. R.; Rostedt, N. K. J.; Ala-Nissila, T. Influence of Nanoparticle Size, Loading, and Shape on the Mechanical Properties of Polymer Nanocomposites. *J. Chem. Phys.* **2012**, *137*, 214901.
(17) Chao, H.; Riggleman, R. A. Effect of Particle Size and Grafting Density on the Mechanical Properties of Polymer Nanocomposites. *Polymer* **2013**, *54*, 5222−5229.
(18) Krishnamurthy, L.-N.; Wagner, N. J.; Mewis, J. Shear Thickening in Polymer Stabilized Colloidal Dispersions. *J. Rheol.* **2005**, *49*, 1347−1360.
(19) Jiang, T.; Zukoski, C. F. Role of Particle Size and Polymer Length in Rheology of Colloid-Polymer Composites. *Macromolecules* **2012**, *45*, 9791−9803.
(20) Shen, J.; Liu, J.; Li, H.; Gao, Y.; Li, X.; Wu, Y.; Zhang, L. Molecular Dynamics Simulations of the Structural, Mechanical and Visco-Elastic Properties of Polymer Nanocomposites Filled with Grafted Nanoparticles. *Phys. Chem. Chem. Phys.* **2015**, *17*, 7196−7207.
(21) Hamming, L. M.; Qiao, R.; Messersmith, P. B.; Catherine Brinson, L. Effects of Dispersion and Interfacial Modification on the Marcoscale Properties of TiO_2 Polymer-Matrix Nanocomposites. *Compos. Sci. Technol.* **2009**, *69*, 1880−1886.
(22) Akcora, P.; Liu, H.; Kumar, S. K.; Moll, J.; Li, Y.; Benicewicz, B. C.; Schadler, L. S.; Acehan, D.; Panagiotopoulos, A. Z.; Pryamitsyn, V.; Ganesan, V.; Ilavsky, J.; Thiyagarajan, P.; Colby, R. H.; Douglas, J. F. Anisotropic self-assembly of spherical polymer-grafted nanoparticles. *Nat. Mater.* **2009**, *8*, 354−359.
(23) Akcora, P.; Kumar, S. K.; García Sakai, V.; Li, Y.; Benicewicz, B. C.; Schadler, L. S. Segmental Dynamics in PMMA-Grafted Nanoparticle Composites. *Macromolecules* **2010**, *43*, 8275−8281.
(24) Corbierre, M. K.; Cameron, N. S.; Sutton, M.; Laaziri, K.; Lennox, R. B. Gold Nanoparticle/Polymer Nanocomposites: Dispersion of Nanoparticles as a Function of Capping Agent Molecular Weight and Grafting Density. *Langmuir* **2005**, *21*, 6063−6072.
(25) Lan, Q.; Francis, L. F.; Bates, F. S. Silica Nanoparticle Dispersions in Homopolymer Versus Block Copolymer. *J. Polym. Sci., Part B: Polym. Phys.* **2007**, *45*, 2284−2299.
(26) Harton, S. E.; Kumar, S. K. Mean-Field Theoretical Analysis of Brush-Coated Nanoparticle Dispersion in Polymer Matrices. *J. Polym. Sci., Part B: Polym. Phys.* **2008**, *46*, 351−358.
(27) Meng, D.; Kumar, S. K.; Cheng, S.; Grest, G. S. Simulating the Miscibility of Nanoparticles and Polymer Melts. *Soft Matter* **2013**, *9*, 5417−5427.
(28) Vrij, A. Polymers at Interfaces and the Interactions in Colloidal Dispersions. *Pure Appl. Chem.* **1976**, *48*, 471−483.
(29) Chabert, E.; Bornert, M.; Bourgeat-Lami, E.; Cavaillé, J.-Y.; Dendievel, R.; Gauthier, C.; Putaux, J. L.; Zaoui, A. Filler-Filler Interactions and Viscoelastic Behavior of Polymer Nanocomposites. *Mater. Sci. Eng., A* **2004**, *381*, 320−330.
(30) Akcora, P.; Kumar, S. K.; Moll, J.; Lewis, S.; Schadler, L. S.; Li, Y.; Benicewicz, B. C.; Sandy, A.; Narayanan, S.; Ilavsky, J.; Thiyagarajan, P.; Colby, R. H.; Douglas, J. F. "Gel-like" Mechanical Reinforcement in Polymer Nanocomposite Melts. *Macromolecules* **2010**, *43*, 1003−1010.
(31) Kim, S. Y.; Meyer, H. W.; Saalwächter, K.; Zukoski, C. F. Polymer Dynamics in PEG-Silica Nanocomposites: Effects of Polymer Molecular Weight, Temperature and Solvent Dilution. *Macromolecules* **2012**, *45*, 4225−4237.
(32) Henderson, D.; Kovalenko, A.; Pizio, O.; Wasan, D. The Effective Interaction between Colloidal Hard Sphere Particles in a Polymerizing Solvent. Application of Wertheim's Theory of Association. *Phys. A* **1997**, *245*, 276−296.
(33) Berriot, J.; Montes, H.; Martin, F.; Mauger, M.; Pyckhout-Hintzen, W.; Meier, G.; Frielinghaus, H. Reinforcement of Model Filled Elastomers: Synthesis and Characterization of the Dispersion State by SANS Measurements. *Polymer* **2003**, *44*, 4909−4919.
(34) Berriot, J.; Montes, H.; Lequeux, F.; Long, D.; Sotta, P. Evidence for the Shift of the Glass Transition near the Particles in Silica-Filled Elastomers. *Macromolecules* **2002**, *35*, 9756−9762.
(35) Liu, J.; Gao, Y.; Cao, D.; Zhang, L.; Guo, Z. Nanoparticle Dispersion and Aggregation in Polymer Nanocomposites: Insights from Molecular Dynamics Simulation. *Langmuir* **2011**, *27*, 7926−7933.
(36) Banc, A.; Genix, A.-C.; Chirat, M.; Dupas, C.; Caillol, S.; Sztucki, M.; Oberdisse, J. Tuning Structure and Rheology of Silica-Latex Nanocomposites with the Molecular Weight of Matrix Chains: A Coupled SAXS-TEM-Simulation Approach. *Macromolecules* **2014**, *47*, 3219−3230.
(37) Jouault, N.; Vallat, P.; Dalmas, F.; Said, S.; Jestin, J.; Boué, F. Well-Dispersed Fractal Aggregates as Filler in Polymer−Silica Nanocomposites: Long-Range Effects in Rheology. *Macromolecules* **2009**, *42*, 2031−2040.
(38) Jouault, N.; Dalmas, F.; Said, S.; Di Cola, E.; Schweins, R.; Jestin, J.; Boué, F. Direct Measurement of Polymer Chain Conformation in Well-Controlled Model Nanocomposites by Combining SANS and SAXS. *Macromolecules* **2010**, *43*, 9881−9891.
(39) Mohite, D. P.; Larimore, Z. J.; Lu, H.; Mang, J. T.; Sotiriou-Leventis, C.; Leventis, N. Monolithic Hierarchical Fractal Assemblies of Silica Nanoparticles Cross-Linked with Polynorbornene via ROMP: A Structure-Property Correlation from Molecular to Bulk through Nano. *Nat. Mater.* **2012**, *24*, 3434−3448.
(40) Baeza, G. P.; Genix, A.-C.; Degrandcourt, C.; Petitjean, L.; Gummel, J.; Couty, M.; Oberdisse, J. Multiscale Filler Structure in Simplified Industrial Nanocomposite Silica/SBR Systems Studied by SAXS and TEM. *Macromolecules* **2013**, *46*, 317−329.
(41) Matinlinna, J. P.; Özcan, M.; Lassila, L. V. J.; Vallittu, P. K. The Effect of a 3-Methacryloxypropyltrimethoxysilane and Vinyltriisopropoxysilane Blend and Tris(3-trimethoxysilylpropyl)isocyanurate on the Shear Bond Strength of Composite Resin to Titanium Metal. *Dent. Mater.* **2004**, *20*, 804−813.
(42) Lin, Y.-C.; Chen, C.-Y.; Chen, H.-L.; Hashimoto, T.; Chen, S.-A.; Li, Y.-C. Hierarchical Self-Assembly of Nanoparticles in Polymer Matrix and the Nature of the Interparticle Interaction. *J. Chem. Phys.* **2015**, *142*, 214905.
(43) Zernike, F.; Prins, J. A. Die Beugung von Röntgenstrahlen in Flüssigkeiten als Effekt der Molekülanordnung. *Z. Phys.* **1927**, *41*, 184−194.
(44) Ornstein, L. S.; Zernike, F. Accidental Deviations of Density and Opalescence at the Critical Point of a Single Substance. *Proc.—Acad. Sci. Amsterdam* **1914**, *17*, 793−807.
(45) Percus, J. K.; Yevick, G. J. Analysis of Classical Statistical Mechanics by Means of Collective Coordinates. *Phys. Rev.* **1958**, *110*, 1−13.
(46) Wertheim, M. S. Exact Solution of the Percus-Yevick Integral Equation for Hard Spheres. *Phys. Rev. Lett.* **1963**, *10*, 321−323.

DOI: 10.1021/acs.macromol.9b00810
Macromolecules 2019, 52, 8312−8322

(47) Kinning, D. J.; Thomas, E. L. Hard-Sphere Interactions between Spherical Domains in Diblock Copolymers. *Macromolecules* **1984**, *17*, 1712−1718.
(48) Chen, S. H.; Lin, T. L. "Neutron Scattering". In *Methods of Experimental Physics Part B*; Skold, K., Price, D. L., Eds.; Academic Press: New York, 1986; Vol. *23*.
(49) Schulz, G. V. On the Relationship between the Rate of Reaction and Composition of the Reaction Products in Macro Polymerization Processes. *Z. Phys. Chem., Abt. B* **1935**, *30*, 379−398.
(50) Hayter, J. B.; Penfold, J. An Analytic Structure Factor for Macroion Solutions. *Mol. Phys.* **1981**, *42*, 109−118.
(51) Guinier, A.; Fournet, G. *Small-Angle Scattering of X-Rays*; John Wiley and Sons: New York, 1955.
(52) Greenwood, R.; Kendall, K. Selection of Suitable Dispersants for Aqueous Suspensions of Zirconia and Titania Powders using Acoustophoresis. *J. Eur. Ceram. Soc.* **1999**, *19*, 479−488.
(53) Balke, S. T.; Hamielec, A. E. Bulk Polymerization of Methyl Methacrylate. *J. Appl. Polym. Sci.* **1973**, *17*, 905−949.
(54) Salami-Kalajahi, M.; Haddadi-Asl, V.; Rahimi-Razin, S.; Behboodi-Sadabad, F.; Roghani-Mamaqani, H.; Hemmati, M. Investigating the effect of pristine and modified silica nanoparticles on the kinetics of methyl methacrylate polymerization. *Chem. Eng. J.* **2011**, *174*, 368−375.
(55) Hooper, J. B.; Schweizer, K. S. Contact Aggregation, Bridging, and Steric Stabilization in Dense Polymer−Particle Mixtures. *Macromolecules* **2005**, *38*, 8858−8869.
(56) Hooper, J. B.; Schweizer, K. S. Theory of Phase Separation in Polymer Nanocomposites. *Macromolecules* **2006**, *39*, 5133−5142.
(57) Rudin, A. *The Elements of Polymer Science and Engineering*; Academic Press: Orlando, FL, 1982; pp 209−211.
(58) Cowie, J. M. G. *Polymers: Chemistry and Physics of Modern Materials*, 2nd ed.; Chapman & Hall: Blackie, USA, 1991; pp 58−60.
(59) Hiemenz, P. C.; Lodge, T. P. *Polymer Chemistry*, 2nd ed.; CRC Press: Boca Raton, FL, 2007; pp 94−96.
(60) Cowie, J. M. G.; Arrighi, V. *Polymers: Chemistry and Physics of Modern Materials*, 3nd ed.; CRC Press: Scotland, 2008.

DOI: 10.1021/acs.macromol.9b00810
Macromolecules 2019, 52, 8312−8322